nature geoscience

LETTERS

PUBLISHED ONLINE: 7 NOVEMBER 2016 | DOI: 10.1038/NGEO2827

Tropospheric ozone change from 1980 to 2010 dominated by equatorward redistribution of emissions

Yuqiang Zhang[1†], Owen R. Cooper[2,3], Audrey Gaudel[2,3], Anne M. Thompson[4], Philippe Nédélec[5], Shin-Ya Ogino[6] and J. Jason West[1*]

Ozone is an important air pollutant at the surface[1], and the third most important anthropogenic greenhouse gas in the troposphere[2]. Since 1980, anthropogenic emissions of ozone precursors—methane, non-methane volatile organic compounds, carbon monoxide and nitrogen oxides (NO_x)—have shifted from developed to developing regions. Emissions have thereby been redistributed equatorwards[3–6], where they are expected to have a stronger effect on the tropospheric ozone burden due to greater convection, reaction rates and NO_x sensitivity[7–11]. Here we use a global chemical transport model to simulate changes in tropospheric ozone concentrations from 1980 to 2010, and to separate the influences of changes in the spatial distribution of global anthropogenic emissions of short-lived pollutants, the magnitude of these emissions, and the global atmospheric methane concentration. We estimate that the increase in ozone burden due to the spatial distribution change slightly exceeds the combined influences of the increased emission magnitude and global methane. Emission increases in Southeast, East and South Asia may be most important for the ozone change, supported by an analysis of statistically significant increases in observed ozone above these regions. The spatial distribution of emissions dominates global tropospheric ozone, suggesting that the future ozone burden will be determined mainly by emissions from low latitudes.

Ozone (O_3) production in the troposphere, by the oxidation of carbon monoxide (CO), non-methane volatile organic compounds (NMVOCs) and methane (CH_4) in the presence of nitrogen oxides (NO_x) and sunlight, exceeds the stratosphere-to-troposphere exchange by a factor of 5–7 (ref. 12). O_3 is an urban and regional air pollutant, but is also sufficiently long-lived (~22 days globally averaged[12]) that its baseline concentrations are elevated over the entire Northern Hemisphere[13] (NH). Observations[14] and models[15,16] have associated emission increases in Asia with increasing O_3 above western North America. The tropospheric O_3 burden (B_{O_3}) is an important quantity that is related to radiative forcing (RF), as O_3 is more effective as a greenhouse gas in the middle and upper troposphere than near the surface[2], and to surface air quality because it influences both urban and rural baseline ozone.

From 1940 to 1980, global anthropogenic emissions of O_3 precursors increased, but the spatial distribution remained fairly unchanged, with the greatest emissions in the NH middle and high latitudes. Starting in 1980, emissions began to shift equatorward as China and low-latitude nations became more industrialized. From 1980 to 2010, global anthropogenic emissions of CO, NO_x and NMVOCs are estimated to have increased by 6.4%, 21.2% and 6.0% (refs 5,17), and the global CH_4 mixing ratio increased by 14.7% (231 ppbv, Methods). During the same period, emissions of CO and NMVOCs increased south of 30° N but decreased north of this latitude, while NO_x emissions increased south of 40° N but decreased to the north (Supplementary Figs 1 and 2).

Here we investigate the influences of global emission changes from 1980 to 2010 on B_{O_3} and surface O_3, separating the influences of changes in: the spatial distribution of anthropogenic short-lived emissions; the global magnitude of emissions; and the global CH_4 mixing ratio. Simulations are conducted with the CAM-chem[18] global chemical transport model for 1980 and 2010, and sensitivity simulations alter these three parameters individually to 1980 conditions, relative to the 2010 simulation (Methods and Supplementary Table 1).

The global B_{O_3} is modelled to have increased by 28.12 Tg (8.9%) from 1980 to 2010 (four-year averages), with 57% of the total increase in the NH (Fig. 1). The largest B_{O_3} increases are over 30° S–30° N (17.93 Tg, Figs 1 and 2). The influence of the change in the spatial distribution of global anthropogenic emissions contributes 16.39 Tg of the total tropospheric O_3 burden change (ΔB_{O_3}), also with a greater influence in the NH than in the Southern Hemisphere (SH), slightly greater than the combined influences of the change in emission magnitude (8.59 Tg) and the global CH_4 change (7.48 Tg) (Fig. 2). The influence of the change in spatial distribution is greater than the sum of the other two influences in three of four years modelled, with the interannual variability in ΔB_{O_3} being much smaller than the overall change (Supplementary Table 2). The sensitivity of B_{O_3} to CH_4 here (0.123 Tg B_{O_3} per Tg CH_4 a^{-1}) is within the range of other models (0.11–0.16 Tg B_{O_3} per Tg CH_4 a^{-1}, ref. 19). Note that the total ΔB_{O_3} from the sum of the three sensitivity simulations (32.46 Tg) is larger than the difference between S_2010 (Supplementary Table 1) and S_1980 (28.12 Tg), as only one variable is changed to 1980 conditions in each simulation. Over 30° S–30° N, the ΔB_{O_3} from the emission spatial distribution change is much greater than the other influences. In extratropical regions, the ΔB_{O_3} from the emission spatial distribution change is only slightly greater or comparable to ΔB_{O_3} from the other influences. North of 60° N, the ΔB_{O_3} due to the emission spatial

[1]Environmental Sciences and Engineering Department, University of North Carolina at Chapel Hill, Chapel Hill, North Carolina 27599, USA. [2]Cooperative Institute for Research in Environmental Sciences, University of Colorado, Boulder, Colorado 80309, USA. [3]Chemical Sciences Division, NOAA Earth System Research Laboratory, Boulder, Colorado 80305, USA. [4]NASA Goddard Space Flight Center, Greenbelt, Maryland 20771, USA. [5]Laboratoire d'Aérologie, CNRS, Université Paul Sabatier Toulouse III, FR-31062 Toulouse, France. [6]Japan Agency for Marine-Earth Science and Technology, Yokosuka 237-0061, Japan. [†]Present address: Environmental Protection Agency, Research Triangle Park, North Carolina 27709, USA. *e-mail: jjwest@email.unc.edu

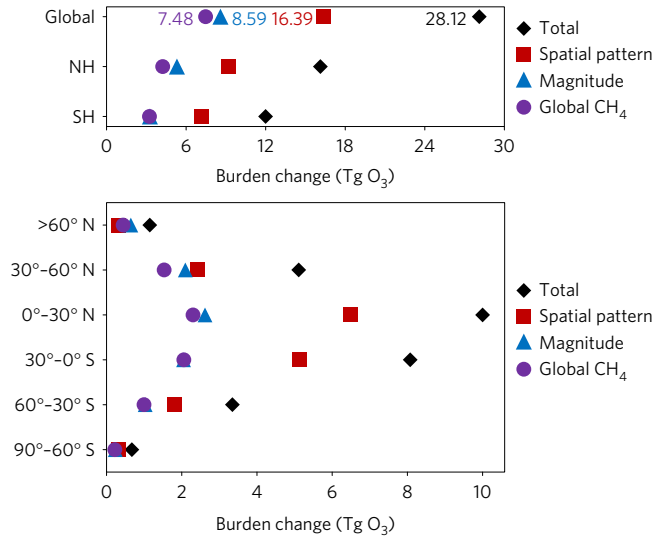

Figure 1 | Tropospheric O_3 burden change (ΔB_{O_3}) from 1980 to 2010. ΔB_{O_3} is shown globally, in each hemisphere, and in different latitudinal bands. The estimated components of ΔB_{O_3} due to the emission spatial distribution change (red square), magnitude change (blue triangle) and global CH_4 change (purple circle) are also seen.

distribution change is lowest, as lower amounts of O_3 and its precursors are transported from North America and Europe.

Between 1980 and 2010, the greatest modelled increases in O_3 burden are over 10°–35° N from the surface to the upper troposphere (Fig. 3). Sixty-eight per cent of ΔB_{O_3} is below 500 hPa, although the greatest changes in mixing ratio are in the middle and upper troposphere (Supplementary Fig. 4). Notable O_3 increases are also seen over 30° S–10° N. Over 35°–60° N, O_3 increases at all altitudes, even though anthropogenic emissions from North America and Europe decreased between 1980 and 2010 (Supplementary Figs 1–3). The influences of the global emission magnitude change and the global CH_4 change both increase O_3 over 30° S–35° N, but the emission spatial distribution change best explains the overall O_3 change, particularly the regions with greatest ozone increases. Increases in O_3 precursor emissions south of 35° N are transported efficiently to the middle and upper troposphere, from strong convection in the Hadley cell, whereas emission decreases north of 35° N stay at high latitudes and low elevation in Ferrell cell circulation (Fig. 4). When global emissions shift equatorward, strong convective mixing over the tropics and subtropics lifts O_3 and its precursor NO_y to higher altitudes (Figs 3b and 4b and Supplementary Figs 4 and 5), where the O_3 lifetime is longer, favouring O_3 accumulation. When emission increases occur in NH mid-latitudes, less NO_y is lofted to high altitudes (Fig. 4c). O_3 increases at high altitudes over middle and high latitudes are affected by the transport of pollutants from the tropics and subtropics[16,20] (Fig. 3b).

In addition to strong convection, the tropics and subtropics have faster chemical reaction rates than other regions (Supplementary Fig. 6), due to the strong sunlight and warm temperatures. Therefore, changes in the O_3 chemical production (P_{O_3}), and loss (L_{O_3}) rates are greater for the spatial distribution change than for the magnitude change, due to greater low-latitude emissions (Supplementary Fig. 7). Similarly, the distribution change increases the global ozone production efficiency, whereas the magnitude change decreases it. In addition, strong NO_x sensitivity prevails over the tropics and subtropics, especially in the middle and upper troposphere (Supplementary Figs 8 and 9), and emission trends show greater increases of NO_x than of NMVOCs (Supplementary Fig. 1). Finally, O_3 lifetime is lower over the tropics, due to destruction from water vapour and dry deposition to vegetated surfaces[20]. However, this effect is clearly not dominant as we see larger O_3 increases over the tropics.

In Fig. 2, the largest modelled ΔB_{O_3} occurs over South and Southeast Asia, suggesting a strong influence of emission increases in these regions. We estimate the importance of different regions for B_{O_3} by multiplying the change in NO_x emissions in each of nine

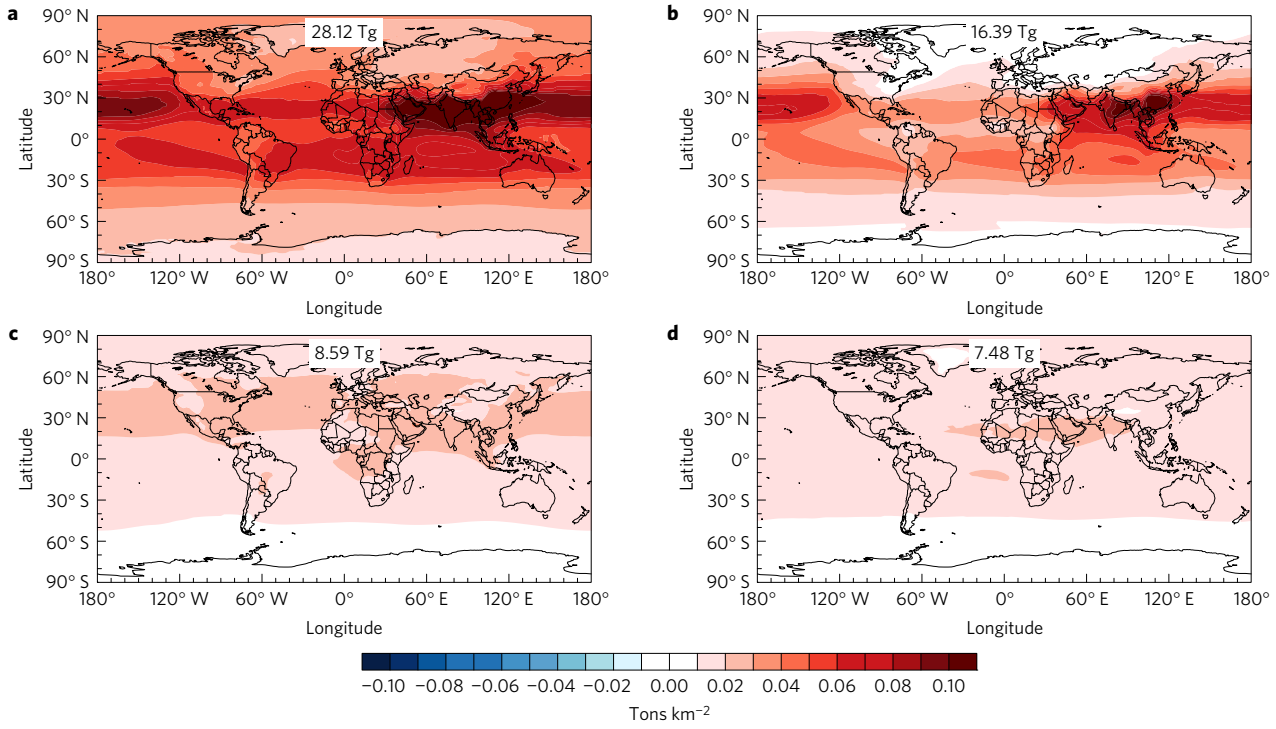

Figure 2 | Spatial distributions for ΔB_{O_3} (tons km^{-2}) from 1980 to 2010. a, Total changes from 1980 to 2010. **b**–**d**, Influences of changes in the global emissions spatial distribution (**b**), the global emissions magnitude (**c**), and global CH_4 mixing ratio (**d**).

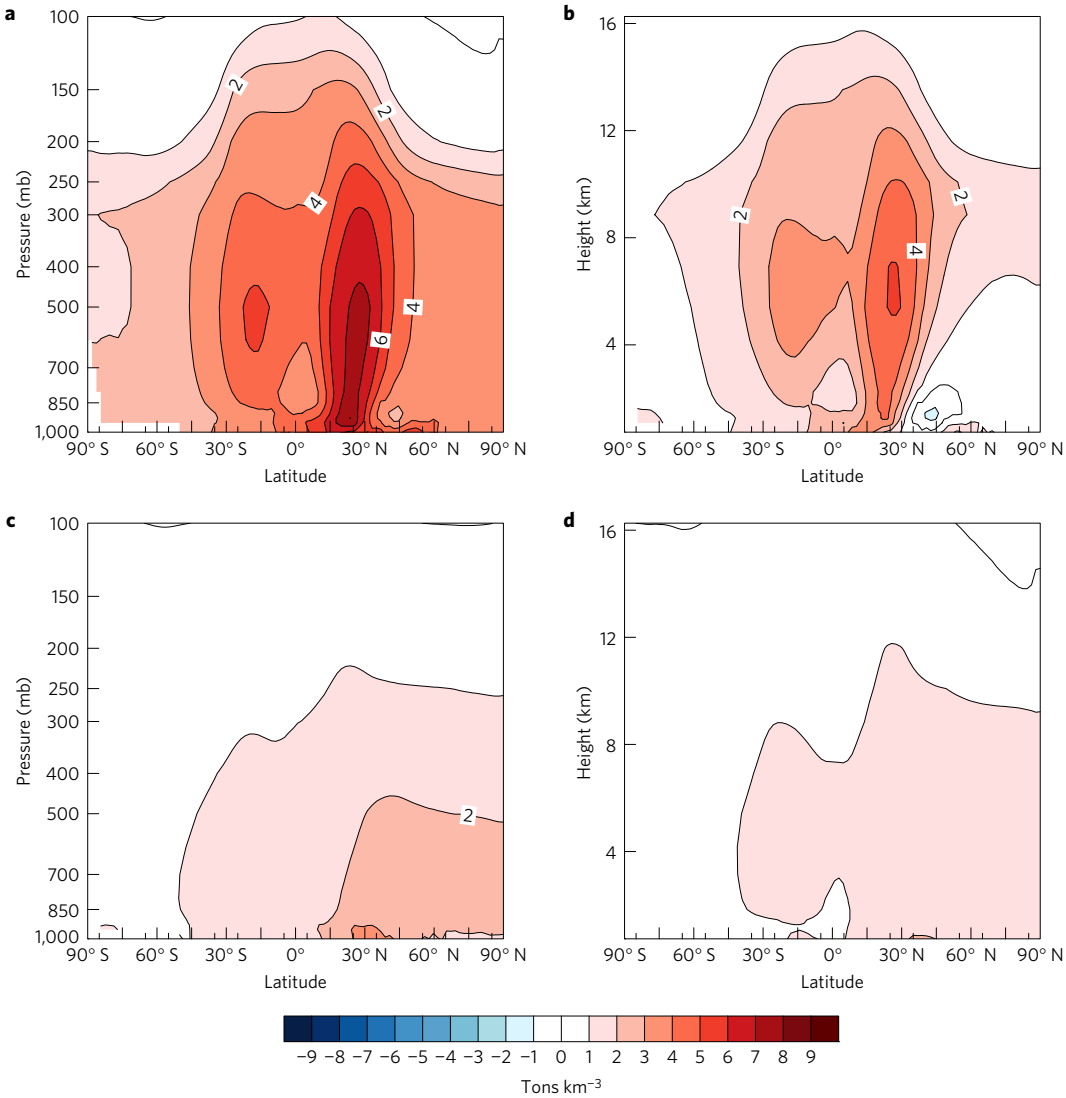

Figure 3 | Zonal annual average O_3 change. a, Total change from 1980 to 2010. **b**–**d**, Influences of changes in the global emissions spatial distribution (**b**), the global emissions magnitude (**c**), and global CH_4 mixing ratio (**d**).

world regions by the sensitivity of B_{O_3} per unit NO_x emissions from ref. 9 (Supplementary Table 3). Doing so, we find that emissions changes from Southeast Asia are most important for the 1980–2010 global ΔB_{O_3}, followed by East Asia and South Asia. Southeast Asia emerges as most important—although its emission increase is only 22% that from East Asia—because of the very large sensitivity of B_{O_3} to NO_x. Strong convection over Southeast Asia contributes to this large sensitivity. Convection over the Himalayas in the NH summer, when the intertropical convergence zone is farthest north, also suggests a pathway for South Asian emissions to the upper troposphere[20] (Supplementary Figs 10 and 11). Future work should model the contributions of emissions changes from each region individually.

Surface O_3 changes, using the three-month O_3-season maximum daily 8-h average O_3 (MDA8) (Supplementary Fig. 12), are dominated by regional emission trends: decreases within Europe and North America, and increases over East and Southeast Asia, consistent with observations[1,21]. Similar regional variations of MDA8 O_3 are also seen from the influence of the global emission spatial pattern change. The MDA8 change between 1980 and 2010 is therefore also dominated by the global emission spatial pattern change, with smaller contributions from the global emission magnitude and CH_4 changes.

These modelled ozone changes are broadly consistent with observed changes over recent decades that show strong increases in South, East and Southeast Asia (Supplementary Information)[21]. In particular, our analyses of ozone observations from IAGOS commercial aircraft[22] and SHADOZ ozonesondes[23] in these regions show good agreement with the model, and changes from 1994–2004 to 2005–2014 that are similar to the modelled 1980–2010 changes (Supplementary Figs 13–15 and Supplementary Table 4); over Southeast Asia and southern India, we show for the first time statistically significant ozone increases at most elevations, whereas for northeastern China, we show that the positive trends detected earlier[24] have continued. We also find that S_1980 compares well with the global ozonesonde climatology of ref. 25, and S_2010 with that of ref. 26 (Supplementary Figs 16 and 17), but is biased high at 200 mb in S_1980 between 30° S and the Equator, and that bias increases in S_2010 between 30° S and 30° N. Given that most of the modelled ΔB_{O_3} is below 500 mb, the bias at 200 mb is probably not very important for our main findings. Comparing the 1980–2010 ozone trends at long-term observation sites, the model overestimates the 1980–2010 ozone change at two of three NH-midlatitude long-term ozonesonde sites (Supplementary Fig. 18), and captures well the 1980–2010 O_3 trend at five of six rural or remote surface sites, although tending to overestimate the trend and to overestimate

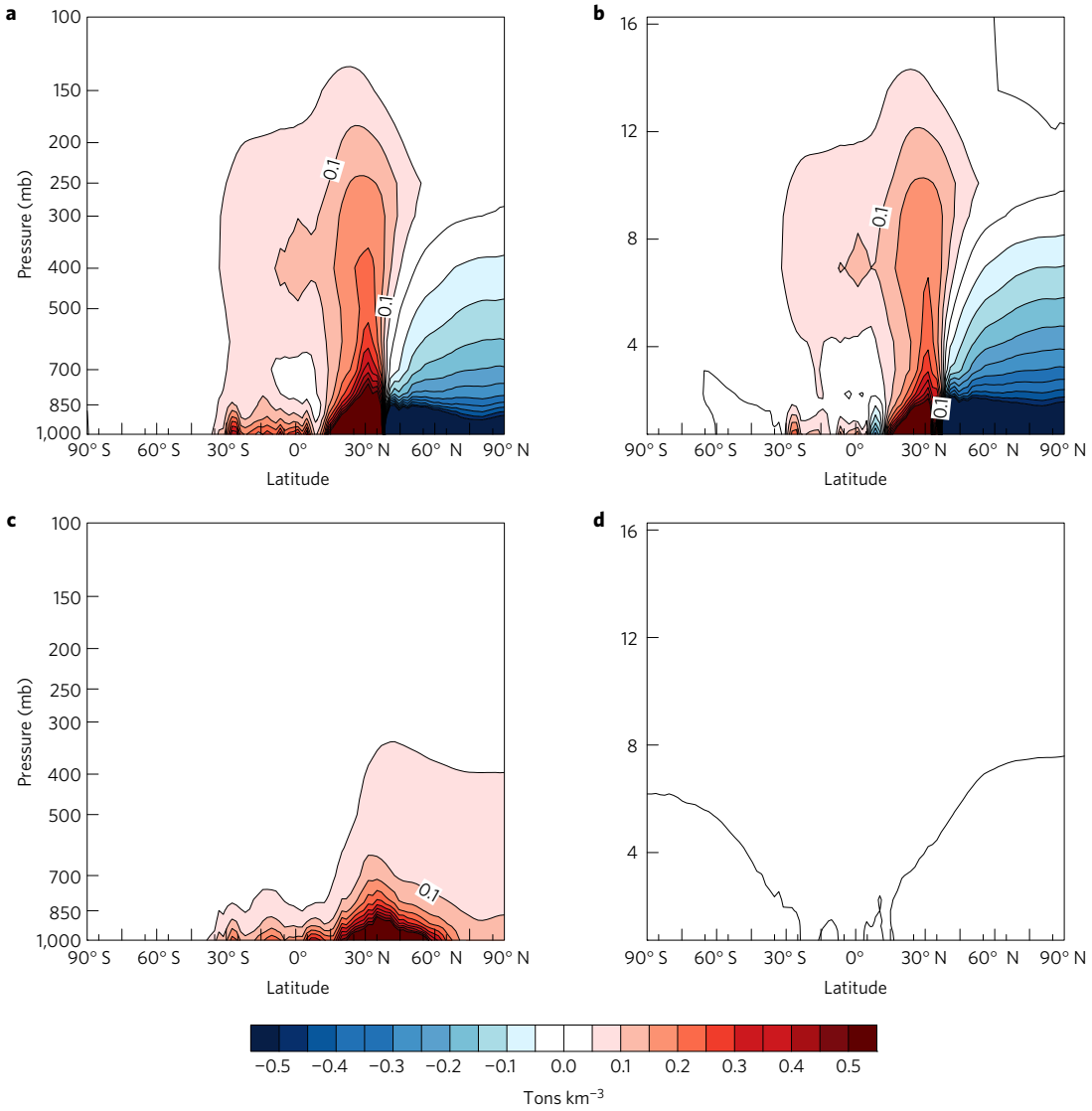

Figure 4 | Zonal annual average NO_y change. a, Total changes from 1980 to 2010. **b**–**d**, Influences of changes in the global emissions spatial distribution (**b**), the global emissions magnitude (**c**), and global CH_4 mixing ratio (**d**). See Methods for the NO_y definition.

O_3 in the NH and underestimate in the SH (Supplementary Fig. 19 and Supplementary Table 5). Compared with OMI/MLS satellite observations[27], S_2010 has high biases for B_{O_3}, particularly in the tropics and subtropics including over Africa (Supplementary Fig. 20), that are comparable to the simulated 1980–2010 burden change (Supplementary Tables 6 and 7), and thus the model may overstate the magnitude of the tropical and subtropical ozone changes. However, OMI/MLS trends in ozone columns from 2004 to 2015 show the greatest growth over South and Southeast Asia (Supplementary Fig. 21), consistent with the model (Fig. 2). Despite model biases, these observations provide strong evidence for ozone increases where the model predicts the greatest increases.

Observations have also shown that the ozone peak has shifted earlier in the year at rural NH sites, and emissions moving equatorward has been hypothesized as an explanation[21,28]. However, S_2010 does not show the observed shift in the timing of ozone peaks relative to S_1980, nor does S_Distribution (Supplementary Fig. 22). Uncertainty in historical emissions and seasonal distributions, or inaccuracies in model chemistry or physics[29], may be the reasons for our inability to explain these observations.

By using the same meteorology in 1980 and 2010, we neglect the possible effects of climate change or climate variability on ΔB_{O_3}. We also evaluate the contributions of each parameter by simulating 1980 conditions for each parameter individually, relative to the 2010 simulation, and ΔB_{O_3} would probably be smaller had we evaluated relative to 1980. However, we expect that the relative contributions would be similar.

These results are expected to have important implications for the RF of O_3. However, increasing NO_x may cause a negative RF, due mainly to decreases in CH_4, and regions with high sensitivity of B_{O_3} to NO_x emissions also have a high sensitivity of CH_4 to NO_x, with the two RFs roughly cancelling over all source regions[7,10]. CO is sufficiently long-lived that the sensitivity of B_{O_3} does not vary strongly with the location of CO emissions[30]. The effect of the equatorward emission shift on RF should be investigated further.

The change in the spatial distribution of the global anthropogenic emissions from 1980 to 2010 dominates the B_{O_3} change, and is slightly greater than the combined effects of changes in the global emission magnitude and global CH_4. In particular, increases in O_3 precursor emissions in the tropics and subtropics significantly influence the global B_{O_3}, and our findings suggest that emissions increases from Southeast, East and South Asia have been most important for the B_{O_3} increase. This can be attributed to the strong photochemical reaction rates, convection and NO_x sensitivity in the

tropics and subtropics. As a result, the global B_{O_3} might continue to increase due to a continued equatorward shift of emissions, even if global anthropogenic emissions remain unchanged or decrease. The location of emissions and the dominant role of emissions from the tropics and subtropics deserve greater emphasis in future research and projections of global tropospheric ozone.

Methods

Methods, including statements of data availability and any associated accession codes and references, are available in the online version of this paper.

Received 29 March 2016; accepted 27 September 2016; published online 7 November 2016

References

1. The Royal Society *Ground-Level Ozone in the 21st Century: Future Trends, Impacts and Policy Implications* (The Royal Society Science Policy, 2008).
2. Myhre, G. *et al*. in *Climate Change 2013: The Physical Science Basis* (eds Stocker, T. F. *et al*.) Ch. 8 (IPCC, Cambridge Univ. Press, 2013).
3. Richter, A., Burrows, J. P., Nüss, H., Granier, C. & Niemeier, U. Increase in tropospheric nitrogen dioxide over China observed from space. *Nature* **437,** 129–132 (2005).
4. Duncan, B. N. *et al*. A space-based, high-resolution view of notable changes in urban NO_x pollution around the world (2005–2014). *J. Geophys. Res.* **121,** 976–996 (2016).
5. Lamarque, J. F. *et al*. Historical (1850–2000) gridded anthropogenic and biomass burning emissions of reactive gases and aerosols: methodology and application. *Atmos. Chem. Phys.* **10,** 7017–7039 (2010).
6. Granier, C. *et al*. Evolution of anthropogenic and biomass burning emissions of air pollutants at global and regional scales during the 1980–2010 period. *Climatic Change* **109,** 163–190 (2011).
7. Naik, V. *et al*. Net radiative forcing due to changes in regional emissions of tropospheric ozone precursors. *J. Geophys. Res.* **110,** D24306 (2005).
8. Derwent, R. G. *et al*. Radiative forcing from surface NO_x emissions: spatial and seasonal variations. *Climatic Change* **88,** 385–401 (2008).
9. West, J. J., Naik, V., Horowitz, L. W. & Fiore, A. M. Effect of regional precursor emission controls on long-range ozone transport—Part 1: short-term changes in ozone air quality. *Atmos. Chem. Phys.* **9,** 6077–6093 (2009).
10. Fry, M. M. *et al*. The influence of ozone precursor emissions from four world regions on tropospheric composition and radiative climate forcing. *J. Geophys. Res.* **117,** D07306 (2012).
11. Gupta, M. L., Cicerone, R. J. & Elliott, S. Perturbation to global tropospheric oxidizing capacity due to latitudinal redistribution of surface sources of NO_x, CH_4 and CO. *Geophys. Res. Lett.* **25,** 3931–3934 (1998).
12. Young, P. J. *et al*. Pre-industrial to end 21st century projections of tropospheric ozone from the Atmospheric Chemistry and Climate Model Intercomparison Project (ACCMIP). *Atmos. Chem. Phys.* **13,** 2063–2090 (2013).
13. *Hemispheric Transport of Air Pollution 2010—Part A Ozone and Particulate Matter* (United Nations Economic Commission for Europe, 2010).
14. Cooper, O. R., Gao, R.-S., Tarasick, D., Leblanc, T. & Sweeney, C. Long-term ozone trends at rural ozone monitoring sites across the United States, 1990–2010. *J. Geophys. Res.* **117,** D22307 (2012).
15. Cooper, O. R., Andrew, O., Parrish, D. D. & Fahey, D. W. Challenges of a lowered U.S. ozone standard. *Science* **348,** 1096–1097 (2015).
16. Verstraeten, W. W. *et al*. Rapid increases in tropospheric ozone production and export from China. *Nat. Geosci.* **8,** 690–695 (2015).
17. Riahi, K. *et al*. RCP 8.5-A scenario of comparatively high greenhouse gas emissions. *Climatic Change* **109,** 33–57 (2011).
18. Lamarque, J.-F. *et al*. CAM-chem: description and evaluation of interactive atmospheric chemistry in the community Earth system model. *Geosci. Model Dev.* **5,** 369–411 (2012).
19. Fiore, A. M., West, J. J., Horowitz, L. W., Naik, V. & Schwarzkopf, M. D. Characterizing the tropospheric ozone response to methane emission controls and the benefits to climate and air quality. *J. Geophys. Res.* **113,** D08307 (2008).
20. Lawrence, M. G., von Kuhlmann, R., Salzmann, M. & Rasch, P. J. The balance of effects of deep convective mixing on tropospheric ozone. *Geophys. Res. Lett.* **30,** 3–6 (2003).
21. Cooper, O. R. *et al*. Global distribution and trends of tropospheric ozone: an observation-based review. *Elementa* **2,** 000029 (2014).
22. Petzold, A. *et al*. Global-scale atmosphere monitoring by in-service aircraft—current achievements and future prospects of the European Research Infrastructure IAGOS. *Tellus B* **67,** 28452 (2015).
23. Thompson, A. M. *et al*. Southern Hemisphere Additional Ozonesondes (SHADOZ) 1998–2004 tropical ozone climatology: 3. Instrumentation, station-to-station variability, and evaluation with simulated flight profiles. *J. Geophys. Res.* **112,** D03304 (2007).
24. Ding, A. J. *et al*. Tropospheric ozone climatology over Beijing: analysis of aircraft data from the MOZAIC program. *Atmos. Chem. Phys.* **8,** 1–13 (2008).
25. Logan, J. A. An analysis of ozonesonde data for the troposphere: recommendations for testing 3-D models and development of a gridded climatology for tropospheric ozone. *J. Geophys. Res.* **104,** 16115–16149 (1999).
26. Tilmes, S. *et al*. Technical note: ozonesonde climatology between 1995 and 2011: description, evaluation and applications. *Atmos. Chem. Phys.* **12,** 7475–7497 (2012).
27. Ziemke, J. R. *et al*. A global climatology of tropospheric and stratospheric ozone derived from Aura OMI and MLS measurements. *Atmos. Chem. Phys.* **11,** 9237–9251 (2011).
28. Parrish, D. *et al*. Lower tropospheric ozone at northern midlatitudes: changing seasonal cycle. *Geophys. Res. Lett.* **40,** 1631–1636 (2013).
29. Parrish, D. D. *et al*. Long-term changes in lower tropospheric baseline ozone concentrations: comparing chemistry-climate models and observations at northern midlatitudes. *J. Geophys. Res.* **119,** 719–5736 (2014).
30. Fry, M. M. *et al*. Net radiative forcing and air quality responses to regional CO emission reductions. *Atmos. Chem. Phys.* **13,** 5381–5399 (2013).

Acknowledgements

Y.Z. and J.J.W. were funded by National Institute of Environmental Health Sciences grant no. 1 R21 ES022600-01 and Environmental Protection Agency STAR grants no. 834285 and RD83587801, and O.R.C. and A.G. were funded by NOAA's Health of the Atmosphere and Atmospheric Chemistry and Climate Programs. The contents are solely the responsibility of the grantee and do not necessarily represent the official views of the US EPA or other funding sources. We thank the NCAR AMWG for developing and maintaining the diagnostic package for the model evaluation. We acknowledge the free use of O_3 observation data from NOAA GMD for the remote sites of Barrow, Mauna Loa, Samoa and South Pole; Global Atmosphere Watch World Data Centre for Greenhouse Gases for Hohenpeissenberg, J. Schwab from University at Albany-SUNY for Whiteface Mountain, and P. Young of Lancaster University for processed ozonesonde climatology of ref. 25.

Author contributions

Y.Z., J.J.W. and O.R.C. designed the study and Y.Z. and J.J.W. planned the model experiments. Y.Z. prepared the emission inputs, performed the model simulations, and prepared the figures. Y.Z. and A.G. conducted data analysis for observations, and J.J.W. and O.R.C. assisted with the data analysis. P.N., S.-Y.O. and A.M.T. provided observational data. Y.Z., J.J.W. and O.R.C. wrote the paper with comments from A.M.T and A.G.

Additional information

Supplementary information is available in the online version of the paper. Reprints and permissions information is available online at www.nature.com/reprints. Correspondence and requests for materials should be addressed to J.J.W.

Competing financial interests

The authors declare no competing financial interests.

Methods

Global emissions spatial pattern change. Here we use anthropogenic emissions including biomass burning in 1980 from the Atmospheric Chemistry and Climate Model Intercomparison Project (ACCMIP, ref. 5), and in 2010 from the representative concentration pathways 8.5 (RCP8.5) scenario[17,31], which are downloaded from the RCP database (http://tntcat.iiasa.ac.at:8787/RcpDb/dsd?Action=htmlpage&page=download, accessed 10/31/2014) to analyse emission trends and drive the global model (Supplementary Figs 1 and 2). RCP8.5 2010 emissions are self-consistent with the ACCMIP historical emissions, and are considered to be the most reasonable scenario to extend ACCMIP emissions beyond 2000 (ref. 6) as they track the GAINS current legislation scenario for several decades[17]. The 2010 global total anthropogenic emissions of CO, NO_x and non-methane volatile organic compounds (NMVOCs) are 1030 Tg, 82 Tg NO and 180 Tg, respectively. As with other global emission estimates for short-lived species, emissions are uncertain and may be especially uncertain in some developing regions[29,32–34]. The rapid growth of emissions in the tropics and subtropics is seen in global emission inventories[5,6] as well as regional ones[35,36]. These inventories are supported by observations from satellites[3,4,37,38] and from surface and airborne observations[29,39] that show that NO_2 in developed regions, such as Europe and North America, have greatly diminished emissions since 1980, but the emissions are increasing in developing countries, especially China and India, shifting global emissions equatorward.

CAM-chem model configuration. We use the global chemistry–climate model CAM-chem, which is based on the global Community Atmosphere Model (CAM) version 4, the atmospheric component of the Community Earth System Model (CESM, v1.2.2) (refs 18,40). The model has a horizontal resolution of 1.9° (latitude) × 2.5° (longitude), and 56 vertical levels between the surface and 4 hPa (≈40 km) with a time step of 1,800 s. We use the NASA Global Modeling and Assimilation Office GEOS-5 meteorology to drive the model as a chemical transport model. For all simulations, we run CAM-chem for five consecutive years, with the first year as spin-up and results are shown as a four-year average. Monthly mean distributions of chemically active stratospheric species (such as O_3, NO, NO_2 and N_2O_5) are prescribed using the climatology from the Whole Atmospheric Community Climate Model simulations[41], following ref. 18. We use a single global chemical transport model, and results with other models may differ, particularly due to different reaction mechanisms.

NMVOC species from ACCMIP (1980) and RCP8.5 (2010) are both re-speciated to match the CAM-chem VOC categories following previous studies[30,42,43]. Monthly temporal variations for all anthropogenic emission sectors are also added based on the monthly time dependence of emissions from RETRO[30,42–44], except for aircraft, shipping and biomass burning for which seasonal variations were provided. The Model of Emissions of Gases and Aerosols from Nature (MEGAN-v2.1, ref. 45) simulates biogenic emissions for 150 compounds online within CAM-chem, yielding four-year average global biogenic emissions of isoprene, monoterpene, methanol and acetone of 420.69 Tg yr^{-1}, 133.23 Tg yr^{-1}, 91.99 Tg yr^{-1} and 42.67 Tg yr^{-1}. Lightning NO_x emissions are calculated online as 3.21 TgN yr^{-1} (four-year average), which is lower than the average of ACCMIP models for 2000, but within the range[12]; lower lightning NO_x emissions may affect the sensitivity of ozone to NO_x and VOCs, particularly in the tropics and mid-troposphere where lightning emissions are greatest. Other natural emissions (ocean, volcano and soil) are from the standard CAM-chem emission files (for 2000), and remain the same for all of the simulations, with soil NO_x at 8.0 TgN yr^{-1} (refs 18,46). The CH_4 volume mixing ratio (ppb) is fixed at uniform global values of 1,567 and 1,798 ppbv for 1980 and 2010 (ref. 47).

In addition to simulating 1980 and 2010, we conduct three sensitivity simulations in which the spatial distribution of global anthropogenic emissions (S_Distribution), the magnitude of the global emissions (S_Magnitude), and the global CH_4 mixing ratio (S_CH_4) are individually set to 1980 levels and all other parameters stay the same as the 2010 simulation (Supplementary Table 1). Here global anthropogenic emissions refer to all short-lived species, including ozone precursors and other species such as aerosols, from anthropogenic sources including biomass burning. The differences between S_2010 and S_1980 reflect the total emission changes from 1980 to 2010. Each of the other three simulations is subtracted from S_2010 to isolate individual influences. We use meteorology from 2009–2012 with 2008 as a spin-up for all simulations, isolating the effects of changes in emissions and neglecting possible effects of climate variability or change from 1980 to 2010.

Tropospheric O_3 burden (B_{O_3}) is defined as the total below the chemical tropopause of 150 ppbv ozone in the S_2010 simulation, with the same tropopause applied to all simulations. The four-year average B_{O_3} in S_2010 is 342.7 Tg, within the range of ACCMIP models (337 ± 23 Tg for 1995–2005), and the 1980–2010 ΔB_{O_3} of 28.12 Tg is similar to the ACCMIP 15 ± 6 Tg for 1980–2000, and 41 ± 12 for 1980–2030 (RCP8.5) (ref. 12). The three-month ozone season average MDA8 is found for the consecutive three-month period with the highest MDA8 in each grid cell. NO_y (total reactive nitrogen) is calculated as $NO + NO_2 + NO_3 + HNO_3 + HO_2NO_2 + 2 \times N_2O_5 + CH_3CO_3NO_2$ (PAN) + $CH_2CCH_3CO_3NO_2$ (MPAN, methacryloyl peroxynitrate) + $CH_2CHCCH_3OOCH_2ONO_2$ ($ISOPNO_3$, peroxy radical from NO_3 + isoprene) from CAM-chem output.

CAM-chem evaluation. A comprehensive evaluation of S_2010 is performed using a present-day climatology of O_3 data from multi-year observations from ozonesondes, satellites, aircraft campaigns, and ground-based observations, compared with the four-year average of CAM-chem output. Our model captures the vertical distribution of O_3 in ozonesondes[26] very well, although it is biased high between 30° S and 30° N, particularly in the upper troposphere (Supplementary Fig. 23 and Supplementary Table 8). The seasonal cycles of O_3 at specific pressure levels from the ozonesonde data are also captured well by the model (Supplementary Fig. 24), with a correlation coefficient between the observed and simulated monthly regional O_3 average that is usually greater than 0.8 (Supplementary Fig. 25). When evaluating model performance with aircraft campaign observations, we focus on the regional average over the campaign areas, and analyse the data at different altitudes. Generally, the model performs better in the NH than the SH (Supplementary Fig. 26 and Supplementary Table 9). When evaluated with multi-year satellite data[27], the model overestimates O_3 between 20° S and 40° N, which is common for global models[12], with a modelled global B_{O_3} that is 23.8 Tg higher (Supplementary Fig. 20). Compared with surface O_3 observations, S_2010 overestimates O_3 by 5.75 ppbv averaged over all stations in the US (Supplementary Fig. 27), and 0.65 ppbv over Europe (Supplementary Fig. 28), but captures well the seasonal cycles.

Code availability. The CAM-chem model code used to perform all the simulations is available at: https://www2.cesm.ucar.edu/models.

The diagnostic package used to perform the model evaluation is developed and maintained by the NCAR AMWG, and code can be found at: https://www2.cesm.ucar.edu/working-groups/amwg/amwg-diagnostics-package/find-code.

Data availability. Hourly O_3 observations for the remote sites of Barrow, Mauna Loa, Samoa and South Pole are maintained by the NOAA Global Monitoring Division (GMD) and can be found at: ftp://aftp.cmdl.noaa.gov/data/ozwv/SurfaceOzone.

Hourly ozone data from Hohenpeissenberg for the years 1971–2010 were downloaded from the Global Atmosphere Watch (GAW) World Data Centre for Greenhouse Gases: http://ds.data.jma.go.jp/gmd/wdcgg. The Meteorological Observatory Hohenpeissenberg is operated and financed by the German Meteorological Service (DWD).

The Whiteface Mountain Summit ozone data were collected by the University at Albany-SUNY with instrumentation provided by the New York State Department of Environmental Conservation. The data set was provided by J. J. Schwab, Atmospheric Sciences Research Center, University at Albany-SUNY, and is archived by the United States Environmental Protection Agency: http://www.epa.gov/ttn/airs/aqsdatamart.

Ozone profiles from commercial aircraft were collected and made freely available by the Measurement of Ozone and water vapour on Airbus In-service airCraft – In-service Aircraft for a Global Observing System (MOZAIC-IAGOS) programme (www.iagos.org). The data were made possible by: the European Commission's support for the MOZAIC project (1994–2003) and the preparatory phase of IAGOS (2005–2012); the partner institutions of the IAGOS Research Infrastructure (FZJ, DLR, MPI, KIT in Germany, CNRS, CNES, Météo-France in France and the University of Manchester in the UK); ETHER (CNES-CNRS/INSU) for hosting the database; and the participating airlines (Lufthansa, Air France, Austrian, China Airlines, Iberia, Cathay Pacific) for the transport free of charge of the instrumentation.

The Hanoi, Vietnam ozonesondes were made freely available by the NASA Southern Hemisphere ADditional OZonesondes (SHADOZ) project[23]. The processed ozonesonde climatology of ref. 25 was shared by P. Young of Lancaster University.

Monthly OMI/MLS tropospheric column ozone data[27] were provided by J. Ziemke, Morgan State University, Baltimore, and downloaded from: http://acd-ext.gsfc.nasa.gov/Data_services/cloud_slice. The OMI/MLS tropospheric column ozone product is derived from the Ozone Monitoring Instrument (OMI) and Microwave Limb Sounder (MLS) remote sensors onboard NASA's polar orbiting Aura satellite. MLS retrievals are the latest available, version 4.2.

The data that support the findings of this study are available from the corresponding author on request.

References

31. Moss, R. H. *et al*. The next generation of scenarios for climate change research and assessment. *Nature* **463,** 747–756 (2010).
32. Schopp, W., Klimont, Z., Suutari, R. & Cofala, J. Uncertainty analysis of emissions estimates in the RAINS integrated assessment model. *Environ. Sci. Policy* **8,** 601–613 (2005).

33. Bond, T. C. *et al*. Historical emissions of black and organic carbon aerosol from energy-related combustion, 1850–2000. *Glob. Biogeochem. Cycles* **21,** GB2018 (2007).
34. Smith, S. J. *et al*. Anthropogenic sulfur dioxide emissions: 1850–2005. *Atmos. Chem. Phys.* **11,** 1101–1116 (2011).
35. Ohara, T. *et al*. An Asian emission inventory of anthropogenic emission sources for the period 1980–2020. *Atmos. Chem. Phys.* **7,** 4419–4444 (2007).
36. Liousse, C., Essamoi, E., Criqui, P., Granier, C. & Rosset, R. Explosive growth in African combustion emissions from 2005 to 2030. *Environ. Res. Lett.* **9,** 035003 (2014).
37. van der A, R. J. *et al*. Trends, seasonal variability and dominant NO_x source derived from a ten year record of NO_2 measured from space. *J. Geophys. Res.* **113,** D04302 (2008).
38. Hilboll, A., Richter, A. & Burrows, J. P. Long-term changes of tropospheric NO_2 over megacities derived from multiple satellite instruments. *Atmos. Chem. Phys.* **13,** 4145–4169 (2013).
39. Thompson, A. M. *et al*. Tropospheric ozone increases over the southern Africa region: bellwether for rapid growth in Southern Hemisphere pollution? *Atmos. Chem. Phys.* **14,** 9855–9869 (2014).
40. Tilmes, S. *et al*. Description and evaluation of tropospheric chemistry and aerosols in the Community Earth System Model (CESM1.2). *Geosci. Model Dev.* **8,** 1395–1426 (2015).
41. Garcia, R. R., Marsh, D. R., Kinnison, D. E., Boville, B. A. & Sassi, F. Simulation of secular trends in the middle atmosphere, 1950–2003. *J. Geophys. Res.* **112,** D09301 (2007).
42. Fry, M. M., Schwarzkopf, M. D., Adelman, Z. & West, J. J. Air quality and radiative forcing impacts of anthropogenic volatile organic compound emissions from ten world regions. *Atmos. Chem. Phys.* **14,** 523–535 (2014).
43. West, J. J. *et al*. Co-benefits of global greenhouse gas mitigation for future air quality and human health. *Nat. Clim. Change* **3,** 885–889 (2013).
44. Schultz, M. G. *et al*. *REanalysis of the TROpospheric Chemical Composition over the Past 40 Years* (*RETRO*)*—A Long-term Global Modeling Study of Tropospheric Chemistry Final Report* (Jülich/Hamburg, Germany, August 2007).
45. Guenther, A. B. *et al*. The model of emissions of gases and aerosols from nature version 2.1 (MEGAN2.1): an extended and updated framework for modeling biogenic emissions. *Geosci. Model Dev.* **5,** 1471–1492 (2012).
46. Emmons, L. K. *et al*. Description and evaluation of the model for ozone and related chemical tracers, version 4 (MOZART-4). *Geosci. Model Dev.* **3,** 43–67 (2010).
47. Prather, M. *et al*. in *Climate Change 2013: The Physical Science Basis* (eds Stocker, T. F. *et al*.) Annex II (IPCC, Cambridge Univ. Press, 2013).